IEEE Access
Multidisciplinary | Rapid Review | Open Access Journal

Received March 29, 2019, accepted April 13, 2019, date of publication April 24, 2019, date of current version May 6, 2019.

Digital Object Identifier 10.1109/ACCESS.2019.2913049

Fault Diagnosis of Analog Filter Circuit Based on Genetic Algorithm

CHENGLIN YANG[1], (Member, IEEE), LIU ZHEN[1], (Member, IEEE), AND CONG HU[2]
[1]School of Automation Engineering, University of Electronic Science and Technology of China, Chengdu 611731, China
[2]Guangxi Key Laboratory of Automatic Detecting Technology and Instruments, Guilin University of Electronic Technology, Guilin 541004, China

Corresponding author: Chenglin Yang (yangclin@uestc.edu.cn)

This work was supported in part by the Open Foundation of the Guangxi Key Laboratory of Automatic Detecting Technology and Instruments under Grant YQ18207, and in part by the National Natural Science Foundation of China under Grant U1830133.

ABSTRACT Hard (open and short) faults and discrete parameter faults (DPFs) are the mostly used fault models in the simulation-before-test (SBT) method. Because the parameter of the analog element is continuous, the DPF cannot elaborately characterize all possible continuous parameter faults (CPF) occurring in the analog circuit. To address such a problem, a genetic algorithm (GA)-based simulation after the test (SAT) fault diagnosis method is proposed in this paper. The fault diagnosis is transformed into an optimization problem. The genes represent the parameter values of potential faulty components. The faulty circuit response is the objective. Our target is to minimize the difference between the actual faulty response and the GA simulated response. The chromosome that minimizes the difference gives the solution. This method does not save all possible faults in advance while it can diagnosis all continuous fault values. The effectiveness of the proposed method is examined by using filter circuit examples.

INDEX TERMS Fault diagnosis, genetic algorithm, optimization.

I. INTRODUCTION

With the increased complexity of the electronics industry, integration level of electronic products has been improved, and the technical requirements for the design and testing of analog circuits are also rapidly increasing. The most widely applied of analog circuit fault diagnosis method is also fault dictionary method, which belongs to pre-test simulation and is mainly used for hard faults and discrete parameter faults. The test point and frequency affect the fault diagnosis accuracy, hence, some literatures [1]–[3] present test frequencies selection methods. Yu et al. [1] present a novel method of generating multi-frequency test stimuli for incipient faults to improve the fault detection accuracy of analog circuits. Applying aliasing measuring algorithm (AMA) to build an aliasing measuring model (AMM) to generate the multi-frequency test stimuli set for incipient faults. By using the concepts of ambiguity set and integer-coded dictionary, Lei and Qin [2] developed a general and accurate method for test point selection. Besides, multi-frequency analysis is also incorporated in the described method. Xie et al. [3] provide a novel method for single and multiple soft fault diagnosis of analog circuit, which employs the information contained in the frequency response function measurements and focuses on finding models of the circuit under test.

Besides the test frequency, the methods of classification affects the fault diagnosis accuracy. The usually used artificial intelligence methods are neural network (NN) and support vector machine (SVM). These methods need feature extraction before the diagnosis. A high-dimensional feature reduction method in [4] is proposed and applied to detect multiple faults in an induction motor linked to a kinematic chain, which has involved a hybrid feature reduction that ensures a good processing of the acquired vibration signals. Some literatures [5]–[9] put forward several fault diagnosis methods based on neural network. It is concerned with the open-circuit fault diagnosis of phase-controlled three-phase full-bridge rectifier by using a sparse auto encoder-based deep neural network(SAE-based DNN) in [5], the depth and hidden neurons of the SAE-based DNN could be regularly determined to extract the features of input signals. The proposed method named dynamic ensemble convolutional neural network is applied to fault diagnosis by intelligent fusion of the multi-level wavelet packet in [6]. A novel fault diagnostic application of Gaussian–Bernoulli deep belief network (GB-DBN) for electronics-rich analog systems is

The associate editor coordinating the review of this manuscript and approving it for publication was Omid Kavehei.

developed which can more effectively capture the high-order semantic features within the raw output signals in [7]. The multiple faults problem in analog circuit can be addressed by using quantum Hopfield neural network in [8]. The fault features are obtained by the wavelet packet analysis and energy calculation. Zhao et al. [9] proposed a deep learning method based on a deep auto-encoder (DAE) network using operational supervisory control and data acquisition (SCADA) data of wind turbines, achieving anomaly detection and fault analysis of wind turbine components. Methods proposed in [10]–[12] are used to solve fault classification problem based on SVM. It proposed a new decision tree approach for analog circuit fault diagnosis using binary support vector machines (BSVMs) that are trained by using different data sets in [10]. The kurtoses and entropies of the output signals are calculated, which is treated as inputs to train SVM used to fault recognition [11]. Zhang et al. [12] applied generalized multiple kernel learning-support vector machine (GMKL-SVM) method and particle swarm optimization (PSO) algorithm to diagnose fault. Tadeusiewicz and Hałgas [13] focused on local parametric fault diagnosis of nonlinear analog integrated circuit designed in a bipolar and CMOS technology. An algorithm is proposed that allows estimating values of the considered set of the parameters. Zhou et al. [14] presented a method for analog circuit parametric faults diagnosis based on matrix eigenvalues. According to the one-to-one correspondence relationship between the matrix elements and fault cases, fault detection and location are achieved by the maximal and minimal eigenvalues as fault signatures.

Some literatures [15], [16] put forward the performance prediction of analog circuits. Vasan et al. [15] presented a method for detecting faulty circuit condition, isolating fault locations, and predicting the remaining useful performance of analog circuits. Through the successive refinement of the circuit's response to a sweep signal, features are extracted for fault diagnosis. The fault diagnostics problem is posed and solved as a pattern recognition problem using kernel methods. From the extracted features, a fault indicator (FI) is developed for failure prognosis. Liu et al. [16] proposed a signal model-based fault coding to monitor the circuit response after being stimulated to perform a fault diagnosis without training a large amount of sample data and fault classifiers. A fault indicator based on comparison between fault codes can describe performance degradation trends.

The multiple faults problem is handled in literatures [17]–[19]. Khanlari and Ehsanian [17] proposed a method for multiple fault diagnosis in moderate-sized analog circuits. Based on this method, a classifier is independently designed for each of the circuit components. Firstly, whole data are clustered by using K means algorithm. Then, samples in each cluster are classified using a new version of KFCM algorithm. Kumar and Singh [18] proposed a new technique based on fuzzy classifier to implement single and multiple soft fault diagnosis in analog electronic circuit. By analyzing the frequency response of the analog circuit under faulty and fault free conditions, the signature of peak gain, frequency and phase associated with peak gain are observed and extracted. Tadeusiewicz and Hałgas [19] offered a method to deal with multiple soft fault in nonlinear analog circuit, which worked with a system of nonlinear algebraic test equations.

Most of the above mentioned analog fault diagnosis method only diagnose DPF. Slope model [20] can deal with continuous parameter single fault in linear circuits, but it requires at least two points. Neural network methods require a large number of Monte Carlo simulations to evaluate neural network parameters. Yang et al. [21] and Tian et al. [22] presented a method based on complex filed fault model can pinpoint much more fault components with less test points and frequencies. In addition, an optimal test frequency selection method by means of test generation and compression is proposed. This method also simply described the theory of multiple faults diagnosis based on complex model.

Methods for the fault diagnosis of analog circuits are usually classified into two main categories, i.e., simulation before test (SBT) and simulation after test (SAT). Most of the mentioned methods fall into the SBT. The main shortcoming of these methods is that plenty of simulations are needed before test. Even though, all the CPF cannot be thoroughly obtained.

To handle such problems, we using the genetic algorithm to simulate the parameter fault in this paper. The fault diagnosis problem is transformed into an optimization problem. It belongs to the SAT. It do not need any simulation before test and all CPF can be diagnosis. This paper is organized as follows. Section II illustrates the previous work and problems to be solved, including fault model, extraction fault feature, selection sensitive frequency and multiple faults problem. Section III describes principle of the proposed multi-frequency diagnosis method. In section IV, the multiple faults diagnosis method in analog circuit is illustrated. In section V, three examples are used to explain proposed method, which are compared with the previous work to verify the effectiveness. Section VI concludes this paper.

II. PROBLEM FORMULATION

The transfer function of a linear filter circuit can be expressed as follows.

$$H\left(s_q, \boldsymbol{p}\right) = \frac{\dot{U}_o}{\dot{U}_i} = \frac{a_n\left(\boldsymbol{p}\right) s_q^n + a_{n-1}\left(\boldsymbol{p}\right) s_q^{n-1} + \cdots + a_1\left(\boldsymbol{p}\right) s_q^1 + a_o\left(\boldsymbol{p}\right)}{b_m\left(\boldsymbol{p}\right) s_q^m + b_{n-1}\left(\boldsymbol{p}\right) s_q^{m-1} + \cdots + b_1\left(\boldsymbol{p}\right) s_q^1 + b_o\left(\boldsymbol{p}\right)}\Bigg|_{s_q = j\omega_q} \tag{1}$$

where $\boldsymbol{p} = [p_1, p_2, \cdots p_K]$ is the potentially faulty parameter vector (k is the number of potential faulty circuit parameters), ω_q is the q^{th} test frequency. Suppose that M_q is the actual measurement value under the q^{th} test frequency, the fault diagnosis can be transferred into a optimization problem as follows.

$$\begin{aligned} &minimize\ E = \|\boldsymbol{H}\left(\boldsymbol{s}, \boldsymbol{p}\right) - \boldsymbol{M}\| \\ &subject\ to\ \boldsymbol{p} > 0 \end{aligned} \tag{2}$$

where $\boldsymbol{H}(\boldsymbol{s},\boldsymbol{p}) = [H(s_1,\boldsymbol{p}), H(s_2,\boldsymbol{p}), \cdots, H(s_T,\boldsymbol{p})]$, $\boldsymbol{M} = [M_1, M_2, \cdots, M_T]$, T is the number of test frequencies. Our object is to find a $\boldsymbol{p}$ that generate the vector $\boldsymbol{H}(\boldsymbol{s},\boldsymbol{p})$ mostly close to $\boldsymbol{M}$ under the specific test frequencies. $\boldsymbol{p}$ is a candidate solution. The basic idea and flow of the proposed method is as follows.

Step1: The actual response vector of the faulty circuit $\dot{U}_{\mathbf{o}} = [\dot{U}_{o1}, \dot{U}_{o2}, \cdots \dot{U}_{oT}]$ under the T test frequencies are measured and $\boldsymbol{M} = \frac{\dot{U}_{\mathbf{o}}}{\dot{U}_{\mathbf{i}}} = \left[\frac{\dot{U}_{\mathbf{o1}}}{\dot{U}_{\mathbf{i1}}}, \frac{\dot{U}_{\mathbf{o2}}}{\dot{U}_{\mathbf{i2}}}, \cdots, \frac{\dot{U}_{\mathbf{oT}}}{\dot{U}_{\mathbf{iT}}}\right] = [M_1, M_2, \cdots, M_T]$, where $\dot{\boldsymbol{U}}_{\mathbf{i}} = [\dot{U}_{i1}, \dot{U}_{i2}, \cdots \dot{U}_{iT}]$ is the vector of input phasor.

Step2: By using the GA to find a $\boldsymbol{p}$ that minimize the E. In $\boldsymbol{p}$, the component value that out of tolerance is the faulty source.

III. PROPOSED GA BASED METHOD

A. PROBLEM EXPRESSION

The chromosome is a real string with the same form as vector $\boldsymbol{p}$. According to Fedi et al. [24], the k components fall into L ambiguity groups, where $L \leq k$. In each group, any component can be chosen as representative fault. For the l^{th} representative fault, the corresponding individual or chromosome is defined as follows.

$$\boldsymbol{x}_{\boldsymbol{i}}^{(\boldsymbol{l})} = \left[x_{i,1}^{(l)}, x_{i,2}^{(l)}, \ldots, x_{i,j}^{(l)}, \ldots, x_{i,k}^{(l)}\right] \tag{3}$$

$$x_{i,j}^{(l)} \in \begin{cases} [0,\infty], & j = l \\ \left[N_{j0} \times 0.95, N_{j0} \times 1.05\right], & j \neq l \end{cases}$$

where N_{j0} is the nominal value of the j^{th} component. We define subpopulation set $S_l = \{\boldsymbol{x}_1^{(l)}, \boldsymbol{x}_2^{(l)}, \cdots, \boldsymbol{x}_i^{(l)}, \cdots, \boldsymbol{x}_{|S_l|}^{(l)}\}$. There are totally L subsets, viz., each representative fault corresponds to a subpopulation set. Hence, $\boldsymbol{x}_i^{(l)}$ is the i^{th} individual in the l^{th} subset. The whole population consists of the subsets, viz., $P = \bigcup_{l=1}^{L} S_l$. The population size is $|P| = \sum_{l=1}^{L} |S_l|$.

B. FRAME OF THE PROPOSED GA

The frequency vector $\boldsymbol{s}$ of stimulation, response $\boldsymbol{M}$ of actual faulty circuit and transfer function $\boldsymbol{H}$ on selected test points are the input of the proposed GA. The output is the individual $\boldsymbol{x}$ or vector $\boldsymbol{p}$ that minimize $\boldsymbol{E}$. The initial population P consist of subsets S_l. Each subset S_l is separately generated in line 1 through 3 in algorithm 1. The i^{th} individual $x_i^{(l)}$ in subset $\boldsymbol{S_l}$ is constrained by formula (3).

C. CROSSOVER AND MUTATION OPERATION

Under the assumption of single fault, the crossover and mutation operations are executed within each subset. It can assure that the representative faulty component varies within faulty range $[\mathbf{0}, \infty]$ and the fault free components vary within the tolerance range $[N_0 \times 0.95, N_0 \times 1.05]$. The chromosome is real code that represent the component value. Hence, the simulated binary crossover (SBX) and polynomial mutation operators [23] (with a relatively larger value of distribution index such as 20) are adopted.

Algorithm 1 Single Fault GA

Input: $\boldsymbol{s} = [s_1, s_2, \cdots s_T]$, $\mathbf{M}$ and $\boldsymbol{H}$
Output: $\boldsymbol{x}$
1: **For** $l = 1$ to L
2: $\quad S_l = \text{Initiallization}()$;
3: **End**
4: $P = \bigcup_{l=1}^{L} S_l$
5: **For** $g = 1$ to $G_{\max}$
6: $\quad$ **For** $l = 1$ to L
7: $\quad\quad S_l = \text{Mating}(S_l)$;
8: $\quad\quad S_l = \text{Variation}(S_l)$;
9: $\quad$ **End**
10: $\quad Q = \bigcup_{l=1}^{L} S_l$;
11: $\quad C = P \cup Q$;
12: $\quad P = \text{Environmental\_selection}(C, \boldsymbol{s}, \boldsymbol{M}, \boldsymbol{H})$;
13: $\quad\quad [S_1, S_2, \cdots S_L] = \text{Sectionalization}(P)$;
14: **End**
15: $\boldsymbol{x} = \text{Best\_selection}(P)$
16: **Return** $\boldsymbol{x}$

D. ENVIRONMENTAL SELECTION

The new generated L subsets are combined with their parent set P to generate a combine set C. Hence, there are totally $|\text{C}| = 2|\text{P}|$ individuals in C. Binary tournament selection is used to select next generation P from set C. The individual with smaller E is more likely to survive.

Algorithm 2 Environmental Selection

Input: C,$\boldsymbol{s}$, $\boldsymbol{M}$, $\boldsymbol{H}$
Output: P
1: The order of the individual in set C is randomly upset, and $P = \emptyset$;
2: **For** $i = 1$ to $|C|$
3: $\quad P = P \cup \left\{\boldsymbol{p}_{\boldsymbol{argmin}(\|\boldsymbol{H}(\boldsymbol{s},\boldsymbol{p}_{2i-1})-\boldsymbol{M}\|, \|\boldsymbol{H}(\boldsymbol{s},\boldsymbol{p}_{2i})-\boldsymbol{M}\|)}\right\}$
4: **End**

E. SECTIONALIZATION

The binary tournament selection is carried out within the whole set C. It means that individuals to be compared might represent different representative fault sources. We need to partition the selected |P| individuals into L sets according to their gene value. The j^{th} individual in P is denoted by symbol $\boldsymbol{p}^{(j)}$. If the l^{th} gene of the individual $\boldsymbol{p}^{(j)}$ is out of the tolerance range, $[0.95N_{l0}, 1.05N_{l0} 0.95\text{N}_{\text{l0}}, 1.05\text{N}_{\text{l0}}]$, then this individual is moved into subset S_l. The algorithm 3 illustrates the sectionalization steps. Once the iterations are finished, the best one is selected from population P in line 12 of algorithm 1.

IV. EXPERIMENTS

The MATLAB is used for implementation of fault diagnosis framework. For the linear CUT, the MATLAB is used for

Algorithm 3 Sectionalization

Input: $P = \left\{\boldsymbol{p}^{(1)}, \boldsymbol{p}^{(2)}, \cdots, \boldsymbol{p}^{(j)}, \cdots, \mathbf{p}^{(|P|)}\right\}$, where $\boldsymbol{p}^{(j)} = \left[p_1^j, p_2^j, \cdots p_K^j\right]$

Output: $S_1, S_2, \cdots S_L$

1: **For** $l = 1$ to L
2: $S_l = \emptyset$;
3: **For** $j = 1$ to $|P|$
4: **If** $p_l^j \in ([0,\ 0.95N_{l0}) \cup [1.05N_{l0},\ \infty))$
5: $S_l = S_l \cup \left\{\mathbf{p}^{(j)}\right\}$;
6: **End**
7: **End**
8: **End**

simulation while the PSPICE is used to simulate the nonlinear CUT. Due to that the slope technique [20] and the circle method [22] can model and diagnose CPS fault, they are selected as comparison methods.

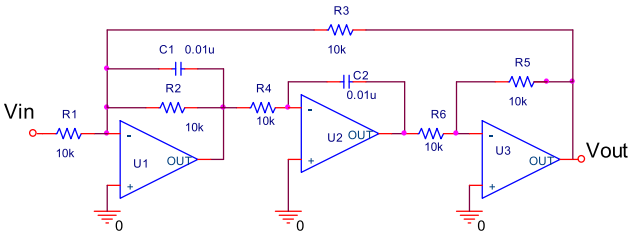

FIGURE 1. Tow–Thomas filter.

A. ILLUSTRATIVE EXAMPLE

This example is mainly used to further illustrate the proposed method. The circuit under test (CUT) is shown in Fig. 1. Where Vout is the test node. The transfer function on Vout is

$$H(j\omega, p) = \frac{\dot{U}_0}{\dot{U}_i} = -\frac{R_2R_3R_6}{R_1R_2R_6 + j\omega R_1R_3R_4R_5C_1 + (j\omega)^2 R_1R_2R_3R_4R_5C_1C_2} \tag{4}$$

TABLE 1. The first generation parent population P.

	R_1	R_2	R_3	R_4	R_5	R_6	C_1	C_2
S_1	**2.682E+02**	9.517E+03	1.037E+04	9.974E+03	9.932E+03	9.818E+03	9.660E-09	1.031E-08
	2.252E+06	1.033E+04	9.570E+03	1.035E+04	1.017E+04	9.741E+03	1.027E-08	1.031E-08
	3.821E+05	9.550E+03	9.923E+03	1.002E+04	9.941E+03	1.036E+04	9.582E-09	1.042E-08
	3.657E+05	9.516E+03	1.012E+04	9.934E+03	9.901E+03	1.001E+04	9.728E-09	1.030E-08
	5.267E+05	1.017E+04	1.032E+04	1.002E+04	9.624E+03	9.700E+03	9.842E-09	1.010E-08
	4.826E+01	1.008E+04	9.692E+03	1.017E+04	1.013E+04	1.026E+04	9.535E-09	9.874E-09
	6.319E+03	9.655E+03	1.046E+04	9.711E+03	9.542E+03	9.547E+03	1.033E-08	9.545E-09
	4.427E+04	1.006E+04	9.680E+03	9.961E+03	9.698E+03	1.013E+04	1.026E-08	1.044E-08
	5.585E+02	9.789E+03	9.712E+03	9.860E+03	1.043E+04	9.734E+03	9.958E-09	9.668E-09
	3.313E+05	9.979E+03	1.021E+04	9.525E+03	9.761E+03	9.655E+03	1.009E-08	1.045E-08
S_2	9.806E+03	**5.233E+06**	9.798E+03	1.010E+04	1.002E+04	9.755E+03	1.046E-08	1.037E-08
	1.038E+04	**2.373E+01**	1.029E+04	1.030E+04	1.031E+04	1.016E+04	1.035E-08	1.019E-08
	1.011E+04	**2.544E+06**	1.025E+04	1.006E+04	9.798E+03	1.006E+04	9.885E-09	1.033E-08
	9.582E+03	**2.472E+05**	9.752E+03	1.021E+04	9.540E+03	9.960E+03	1.018E-08	1.016E-08
	9.682E+03	**5.702E+06**	9.706E+03	9.921E+03	1.028E+04	9.814E+03	1.049E-08	9.541E-09
	1.028E+04	**2.330E+04**	1.011E+04	1.050E+04	9.706E+03	9.949E+03	1.023E-08	1.027E-08
	1.028E+04	**1.165E+04**	9.621E+03	9.643E+03	9.641E+03	9.920E+03	9.892E-09	9.916E-09
	1.031E+04	**2.894E+05**	1.039E+04	1.012E+04	9.655E+03	1.037E+04	9.918E-09	9.679E-09
	1.015E+04	**5.464E+05**	9.557E+03	1.041E+04	9.976E+03	1.047E+04	1.034E-08	9.557E-09
	1.039E+04	**4.013E+06**	9.809E+03	1.006E+04	9.846E+03	9.991E+03	9.903E-09	1.004E-08
S_3	1.040E+04	9.724E+03	**5.087E+06**	1.003E+04	9.654E+03	1.024E+04	9.740E-09	1.027E-08
	1.040E+04	9.885E+03	**3.840E+03**	9.966E+03	9.710E+03	9.871E+03	1.006E-08	1.008E-08
	9.804E+03	9.629E+03	**6.041E+03**	1.007E+04	1.017E+04	9.984E+03	9.664E-09	1.038E-08
	9.727E+03	9.721E+03	**7.356E+01**	9.678E+03	1.038E+04	1.002E+04	9.700E-09	9.855E-09
	9.793E+03	1.032E+04	**6.677E+06**	9.613E+03	1.045E+04	1.014E+04	1.027E-08	9.564E-09
	1.015E+04	1.008E+04	**1.142E+01**	9.915E+03	1.024E+04	9.917E+03	9.606E-09	1.039E-08
	1.003E+04	9.970E+03	**1.144E+05**	1.004E+04	1.022E+04	1.039E+04	9.670E-09	1.039E-08
	9.974E+03	1.047E+04	**1.771E+06**	9.882E+03	9.512E+03	9.824E+03	1.011E-08	9.697E-09
	1.023E+04	1.044E+04	**3.382E+05**	9.608E+03	1.004E+04	9.555E+03	9.536E-09	9.954E-09
	9.843E+03	1.020E+04	**2.029E+04**	1.038E+04	9.662E+03	1.037E+04	1.006E-08	1.021E-08
S_4	1.003E+04	9.939E+03	9.806E+03	**1.224E+04**	1.011E+04	9.748E+03	1.048E-08	1.028E-08
	9.696E+03	1.024E+04	1.018E+04	**8.571E+03**	1.017E+04	1.024E+04	1.015E-08	9.803E-09
	9.684E+03	1.022E+04	9.770E+03	**4.216E+02**	9.986E+03	1.042E+04	9.753E-09	1.008E-08
	9.913E+03	9.809E+03	9.887E+03	**6.015E+03**	1.031E+04	1.040E+04	1.011E-08	9.807E-09
	9.894E+03	1.015E+04	1.042E+04	**4.974E+06**	1.033E+04	1.008E+04	1.030E-08	1.014E-08
	9.908E+03	1.007E+04	1.003E+04	**9.531E+06**	1.041E+04	1.041E+04	9.738E-09	1.026E-08
	9.567E+03	1.002E+04	9.529E+03	**5.275E+04**	1.038E+04	9.994E+03	9.993E-09	9.870E-09
	9.918E+03	9.593E+03	1.031E+04	**1.161E+02**	9.708E+03	1.029E+04	9.650E-09	1.027E-08
	1.003E+04	1.006E+04	9.857E+03	**2.110E+06**	9.685E+03	1.003E+04	1.005E-08	9.928E-09
	9.847E+03	1.040E+04	1.043E+04	**6.261E+05**	1.009E+04	1.004E+04	1.016E-08	1.011E-08

TABLE 2. The first generation child population Q.

	R_1	R_2	R_3	R_4	R_5	R_6	C_1	C_2
S_1	**4.548E+05**	9.501E+03	1.039E+04	9.983E+03	9.917E+03	9.825E+03	9.576E-09	1.035E-08
	1.109E+04	1.018E+04	1.031E+04	1.002E+04	9.614E+03	9.678E+03	9.806E-09	1.018E-08
	9.228E+04	1.036E+04	9.560E+03	1.042E+04	1.025E+04	9.700E+03	1.025E-08	1.039E-08
	1.934E+06	1.006E+04	9.783E+03	9.970E+03	9.662E+03	1.011E+04	1.026E-08	1.042E-08
	7.809E+03	9.797E+03	9.712E+03	9.856E+03	1.047E+04	9.673E+03	1.008E-08	1.046E-08
	4.355E+05	9.943E+03	1.022E+04	9.532E+03	9.751E+03	9.749E+03	9.923E-09	9.661E-09
	6.173E+05	9.513E+03	9.861E+03	1.000E+04	9.967E+03	1.031E+04	9.593E-09	9.884E-09
	3.064E+01	1.010E+04	9.726E+03	1.016E+04	1.020E+04	1.022E+04	9.576E-09	1.037E-08
	1.940E+05	9.572E+03	1.046E+04	9.735E+03	9.551E+03	9.608E+03	1.033E-08	9.537E-09
	8.851E+05	9.588E+03	1.010E+04	9.912E+03	9.900E+03	9.997E+03	9.715E-09	1.032E-08
S_2	1.025E+04	**4.415E+05**	1.012E+04	1.048E+04	9.985E+03	9.774E+03	1.047E-08	1.029E-08
	9.769E+03	**5.525E+06**	9.737E+03	1.014E+04	9.679E+03	9.963E+03	1.027E-08	1.026E-08
	1.017E+04	**1.671E+05**	9.575E+03	1.047E+04	1.002E+04	1.003E+04	1.014E-08	1.016E-08
	9.569E+03	**4.396E+05**	9.734E+03	1.018E+04	9.527E+03	1.050E+04	1.033E-08	9.521E-09
	1.012E+04	**2.204E+06**	1.030E+04	1.005E+04	9.785E+03	1.009E+04	9.902E-09	1.033E-08
	1.044E+04	**4.152E+06**	9.811E+03	1.004E+04	9.837E+03	9.877E+03	9.941E-09	1.006E-08
	1.041E+04	**1.446E+01**	1.029E+04	1.031E+04	1.034E+04	1.016E+04	9.903E-09	9.669E-09
	1.030E+04	**5.118E+05**	1.040E+04	1.015E+04	9.575E+03	1.039E+04	1.035E-08	1.020E-08
	9.655E+03	**5.916E+06**	9.710E+03	9.874E+03	1.036E+04	9.927E+03	9.895E-09	9.919E-09
	1.030E+04	**6.730E+03**	9.593E+03	9.639E+03	9.634E+03	9.803E+03	1.046E-08	9.510E-09
S_3	1.010E+04	9.970E+03	**2.478E+05**	1.003E+04	1.021E+04	1.001E+04	9.686E-09	1.039E-08
	9.822E+03	9.625E+03	**3.597E+04**	1.007E+04	1.015E+04	1.033E+04	9.678E-09	1.033E-08
	1.036E+04	9.949E+03	**7.162E+04**	1.004E+04	9.664E+03	1.024E+04	9.758E-09	1.023E-08
	1.043E+04	9.697E+03	**5.354E+06**	9.969E+03	9.702E+03	9.972E+03	1.007E-08	1.005E-08
	1.001E+04	1.050E+04	**2.123E+06**	9.931E+03	9.523E+03	9.848E+03	1.010E-08	9.687E-09
	9.744E+03	1.032E+04	**6.535E+06**	9.640E+03	1.046E+04	1.014E+04	1.024E-08	9.614E-09
	1.016E+04	9.998E+03	**1.072E+01**	9.899E+03	1.024E+04	9.886E+03	1.007E-08	1.012E-08
	9.916E+03	1.020E+04	**7.332E+02**	1.042E+04	9.660E+03	1.044E+04	9.587E-09	1.033E-08
	1.022E+04	1.045E+04	**1.750E+05**	9.625E+03	1.001E+04	9.574E+03	9.513E-09	9.978E-09
	9.730E+03	9.670E+03	**3.744E+01**	9.765E+03	1.030E+04	1.003E+04	9.646E-09	9.862E-09
S_4	9.824E+03	9.810E+03	9.948E+03	**1.560E+06**	9.675E+03	9.980E+03	1.007E-08	9.928E-09
	1.004E+04	1.007E+04	9.902E+03	**4.345E+03**	1.032E+04	1.040E+04	1.012E-08	9.817E-09
	9.735E+03	1.023E+04	9.833E+03	**1.253E+02**	9.953E+03	1.021E+04	1.014E-08	9.816E-09
	9.667E+03	1.023E+04	1.015E+04	**7.498E+03**	1.015E+04	1.033E+04	9.760E-09	1.008E-08
	9.947E+03	9.982E+03	1.009E+04	**9.630E+06**	1.034E+04	1.025E+04	9.571E-09	1.021E-08
	9.918E+03	9.655E+03	1.029E+04	**1.552E+01**	9.661E+03	1.030E+04	9.716E-09	1.027E-08
	9.548E+03	1.007E+04	9.500E+03	**5.436E+05**	1.041E+04	9.994E+03	1.048E-08	1.033E-08
	1.005E+04	9.957E+03	9.792E+03	**1.018E+06**	1.008E+04	9.752E+03	9.953E-09	9.876E-09
	9.896E+03	1.036E+04	1.039E+04	**4.584E+06**	1.033E+04	1.001E+04	1.027E-08	1.015E-08
	9.903E+03	1.013E+04	1.048E+04	**7.991E+05**	1.009E+04	1.011E+04	1.017E-08	1.006E-08

where, $\boldsymbol{p} = [p_1, p_2, p_3, p_4, p_5, p_6, p_7, p_8,] = [R_1, R_2, R_3, R_4, R_5, R_6, C_1, C_2,]p[p_1, p_2, p_3, p_4, p_5, p_6, p_7, p_8,] = [R_1, R_2, R_3, R_4, R_5, R_6, C_1, C_2,]$. The nominal parameters are shown in this figure. According to the method in [24], the six resistances and two capacitances fall into four ambiguity sets: {R1}, {R2}, {R4, R5, R6, C2}, {R3, C1}. Any component in each set can be chosen as representative fault source. Hence, R1, R2, R3 and R4 are selected in this example. Their tolerance range is [9500Ω, 10500Ω]. The excitation (input) signal is a 1V sinusoidal wave with randomly selected frequencies 500, 1000 and 1500Hz. Proper test frequencies will increase the fault diagnosis accuracy. Theoretically, more frequency number will increase the fault diagnosis accuracy. The optimal frequency selection is out of the range of this paper. The faulty response is simulated by using MATLAB. We set the faulty parameter vector $\boldsymbol{p}$ = [10452Ω, 20000Ω, 9590Ω, 10469Ω, 10207Ω, 9738Ω, 9.6988nF, 9.9735nF]. Obviously, $R_2 = 20000\Omega$ is the faulty component. The other components are all in the tolerance range. With the stimulations of three sinusoidal waves, the responses are $\dot{U}_0\dot{U}_0$ = [−0.9869 + j0.1809V, −1.1765 + j0.6485V, −0.3464+j1.7880V]. Take the inputs as reference phasor, viz., $\dot{U}_i\dot{U}_0$ = [1V, 1V, 1V], we have $\boldsymbol{H_M} = \frac{\dot{U}_0}{\dot{U}_i}$ = [−0.9869+j0.1809]. Our task is to find the faulty component by using the $\boldsymbol{H_M}$ and transfer function (4).

B. INITIALIZATION

There are four subsets respectively represent four representative faults R1, R2, R3 and R4. The size of population for each subsets is 10. They are initialized by using formula (3). Table 1 lists individuals for each subset. The second row of this table lists the first individual $\boldsymbol{x}_1^{(1)}$ = {268.2Ω, 9517Ω,10370Ω,9974Ω,9932Ω, 9818Ω, 9.660nF, 10.31nF} in set S_1. The third row of S_2 shows the third individual $\boldsymbol{x}_3^{(2)}$ = {10110Ω, 2544234Ω, 10251Ω, 10065Ω, 9798Ω, 10067Ω, 9.885nF, 10.33nF}. The elements in second column of the Table 1 within subset S_1 show the value of resistance R_1. It's value varies from 0 to ∞ under the constraint formula (3).

TABLE 3. The selected population.

R_1	R_2	R_3	R_4	R_5	R_6	C_1	C_2
9.655E+03	**5.916E+06**	9.710E+03	9.874E+03	1.036E+04	9.927E+03	9.895E-09	9.919E-09
6.319E+03	9.655E+03	1.046E+04	9.711E+03	9.542E+03	9.547E+03	1.033E-08	9.545E-09
8.851E+05	9.588E+03	1.010E+04	9.912E+03	9.900E+03	9.997E+03	9.715E-09	1.032E-08
1.109E+04	1.018E+04	1.031E+04	1.002E+04	9.614E+03	9.678E+03	9.806E-09	1.018E-08
9.806E+03	**5.233E+06**	9.798E+03	1.010E+04	1.002E+04	9.755E+03	1.046E-08	1.037E-08
1.028E+04	1.165E+04	9.621E+03	9.643E+03	9.641E+03	9.920E+03	9.892E-09	9.916E-09
9.822E+03	9.625E+03	**3.597E+04**	1.007E+04	1.015E+04	1.033E+04	9.678E-09	1.033E-08
4.427E+04	1.006E+04	9.680E+03	9.961E+03	9.698E+03	1.013E+04	1.026E-08	1.044E-08
1.022E+04	1.045E+04	**1.750E+05**	9.625E+03	1.001E+04	9.574E+03	9.513E-09	9.978E-09
1.030E+04	**6.730E+03**	9.593E+03	9.639E+03	9.634E+03	9.803E+03	1.046E-08	9.510E-09
9.894E+03	1.015E+04	1.042E+04	**4.974E+06**	1.033E+04	1.008E+04	1.030E-08	1.014E-08
9.918E+03	9.593E+03	1.031E+04	**1.161E+02**	9.708E+03	1.029E+04	9.650E-09	1.027E-08
1.040E+04	9.885E+03	**3.840E+03**	9.966E+03	9.710E+03	9.871E+03	1.006E-08	1.008E-08
9.744E+03	1.032E+04	**6.535E+06**	9.640E+03	1.046E+04	1.014E+04	1.024E-08	9.614E-09
1.003E+04	9.939E+03	9.806E+03	**1.224E+04**	1.011E+04	9.748E+03	1.048E-08	1.028E-08
9.667E+03	1.023E+04	1.015E+04	**7.498E+03**	1.015E+04	1.033E+04	9.760E-09	1.008E-08
9.913E+03	9.809E+03	9.887E+03	**6.015E+03**	1.031E+04	1.040E+04	1.011E-08	9.807E-09
9.793E+03	1.032E+04	**6.677E+06**	9.613E+03	1.045E+04	1.014E+04	1.027E-08	9.564E-09
9.918E+03	9.655E+03	1.029E+04	**1.552E+01**	9.661E+03	1.030E+04	9.716E-09	1.027E-08
1.934E+06	1.006E+04	9.783E+03	9.970E+03	9.662E+03	1.011E+04	1.026E-08	1.042E-08
6.173E+05	9.513E+03	9.861E+03	1.000E+04	9.967E+03	1.031E+04	9.593E-09	9.884E-09
9.684E+03	1.022E+04	9.770E+03	**4.216E+02**	9.986E+03	1.042E+04	9.753E-09	1.008E-08
1.005E+04	9.957E+03	9.792E+03	**1.018E+06**	1.008E+04	9.752E+03	9.953E-09	9.876E-09
7.809E+03	9.797E+03	9.712E+03	9.856E+03	1.047E+04	9.673E+03	1.008E-08	1.046E-08
4.548E+05	9.501E+03	1.039E+04	9.983E+03	9.917E+03	9.825E+03	9.576E-09	1.035E-08
1.004E+04	1.007E+04	9.902E+03	**4.345E+03**	1.032E+04	1.040E+04	1.012E-08	9.817E-09
1.028E+04	**2.330E+04**	1.011E+04	1.050E+04	9.706E+03	9.949E+03	1.023E-08	1.027E-08
9.548E+03	1.007E+04	9.500E+03	**5.436E+05**	1.041E+04	9.994E+03	1.048E-08	1.033E-08
9.696E+03	1.024E+04	1.018E+04	**8.571E+03**	1.017E+04	1.024E+04	1.015E-08	9.803E-09
9.567E+03	1.002E+04	9.529E+03	**5.275E+04**	1.038E+04	9.994E+03	9.993E-09	9.870E-09
9.727E+03	9.721E+03	**7.356E+01**	9.678E+03	1.038E+04	1.002E+04	9.700E-09	9.855E-09
9.947E+03	9.982E+03	1.009E+04	**9.630E+06**	1.034E+04	1.025E+04	9.571E-09	1.021E-08
3.821E+05	9.550E+03	9.923E+03	1.002E+04	9.941E+03	1.036E+04	9.582E-09	1.042E-08
9.847E+03	1.040E+04	1.043E+04	**6.261E+05**	1.009E+04	1.004E+04	1.016E-08	1.011E-08
1.003E+04	1.006E+04	9.857E+03	**2.110E+06**	9.685E+03	1.003E+04	1.005E-08	9.928E-09
1.040E+04	9.724E+03	**5.087E+06**	1.003E+04	9.654E+03	1.024E+04	9.740E-09	1.027E-08
9.730E+03	9.670E+03	**3.744E+01**	9.765E+03	1.030E+04	1.003E+04	9.646E-09	9.862E-09
9.843E+03	1.020E+04	**2.029E+04**	1.038E+04	9.662E+03	1.037E+04	1.006E-08	1.021E-08
9.804E+03	9.629E+03	**6.041E+03**	1.007E+04	1.017E+04	9.984E+03	9.664E-09	1.038E-08
1.016E+04	9.998E+03	**1.072E+01**	9.899E+03	1.024E+04	9.886E+03	1.007E-08	1.012E-08

All the other components vary within their tolerance range. Similarly, only the third component (the fourth column) is the faulty source and can vary from 0 to ∞ in subset S_3. The maximum generation is 100. The mutation rate is $p_r = 1$ and mutation rate is $p_m = 0.5$. The crossover and mutation operations are executed in each subset respectively.

Table 2 lists the generated population Q. Combine set C is easily obtained by combining the sets P and Q. Then the order of individuals in set C are randomly upset. From the 80 individuals, binary tournament shown in Algorithm 2 is used to choose the next 40 individuals. The results are listed in Table 3.

In Table 3, the first selected individual $\boldsymbol{p}^{(1)} = \{9.655\text{E} + 03, 5.916\text{E} + 06, 9.710\text{E} + 03, 9.874\text{E} + 03, 1.036\text{E} + 04, 9.927\text{E} + 03, 9.895\text{E} - 09, 9.919\text{E} - 09\}$ comes from the ninth individual of subset S_2 in population Q shown in Table 2. The next step is to partition the selected population in Table 3 into four subsets by using the sectionalization Algorithm 3. The results are shown in Table 4. It shows that some subset such as S_2 shrink. Its size decreases from 10 (see Table 1) to 5 (Table 4). While the population size of S_2 increases to 15. The whole population size of P is still 40.

The algorithm then enters the second iteration. After 100 iterations, the final 40 individuals are shown in Table 5. It can be seen that subsets S1, S3, and S4 have no individuals. All individuals belong to S2. The 15$^{\text{th}}$ individual shown in the 16$^{\text{th}}$ row of Table 5 is the best solution. With the parameters $\boldsymbol{p}* = [1.042\text{E} + 04\Omega, 1.818\text{E}+04\Omega, 9.766\text{E}+03\Omega, 9.821\text{E}+03\Omega, 1.045\text{E}+04\Omega, 1.028\text{E} + 04\Omega, 1.017\text{E} - 08\text{F}, 1.016\text{E} - 08\text{F}]$ and 500 Hz, 1000 Hz and 1500Hz stimulations, it is easy to verify that the response of the CUT is $\dot{\boldsymbol{U}}'_{\boldsymbol{o}} = [-1.0044 + j0.1908\text{V}, -1.1763 + \text{j}0.6684\text{V}, -0.3585 + \text{j}1.7524\text{V}]$. Hence $\boldsymbol{H}'_{\boldsymbol{M}} = [-1.0044 + j0.1908, -1.1763 + j0.6684, -0.3585 + j1.7524]$. It is close to the $\boldsymbol{H}_{\boldsymbol{M}} = [-0.9869 + \text{j}0.1809, -1.1765 + \text{j}0.6485, -0.3464 + \text{j}1.7880]$. Obviously,

TABLE 4. The second generation parent P.

	R_1	R_2	R_3	R_4	R_5	R_6	C_1	C_2
S_1	**6.319E+03**	9.655E+03	1.046E+04	9.711E+03	9.542E+03	9.547E+03	1.033E-08	9.545E-09
	8.851E+05	9.588E+03	1.010E+04	9.912E+03	9.900E+03	9.997E+03	9.715E-09	1.032E-08
	1.109E+04	1.018E+04	1.031E+04	1.002E+04	9.614E+03	9.678E+03	9.806E-09	1.018E-08
	4.427E+04	1.006E+04	9.680E+03	9.961E+03	9.698E+03	1.013E+04	1.026E-08	1.044E-08
	1.934E+06	1.006E+04	9.783E+03	9.970E+03	9.662E+03	1.011E+04	1.026E-08	1.042E-08
	6.173E+05	9.513E+03	9.861E+03	1.000E+04	9.967E+03	1.031E+04	9.593E-09	9.884E-09
	7.809E+03	9.797E+03	9.712E+03	9.856E+03	1.047E+04	9.673E+03	1.008E-08	1.046E-08
	4.548E+05	9.501E+03	1.039E+04	9.983E+03	9.917E+03	9.825E+03	9.576E-09	1.035E-08
	3.821E+05	9.550E+03	9.923E+03	1.002E+04	9.941E+03	1.036E+04	9.582E-09	1.042E-08
S_2	9.655E+03	**5.916E+06**	9.710E+03	9.874E+03	1.036E+04	9.927E+03	9.895E-09	9.919E-09
	9.806E+03	**5.233E+06**	9.798E+03	1.010E+04	1.002E+04	9.755E+03	1.046E-08	1.037E-08
	1.028E+04	**1.165E+04**	9.621E+03	9.643E+03	9.641E+03	9.920E+03	9.892E-09	9.916E-09
	1.030E+04	**6.730E+03**	9.593E+03	9.639E+03	9.634E+03	9.803E+03	1.046E-08	9.510E-09
	1.028E+04	**2.330E+04**	1.011E+04	1.050E+04	9.706E+03	9.949E+03	1.023E-08	1.027E-08
S_3	1.040E+04	9.885E+03	**3.840E+03**	9.966E+03	9.710E+03	9.871E+03	1.006E-08	1.008E-08
	9.744E+03	1.032E+04	**6.535E+06**	9.640E+03	1.046E+04	1.014E+04	1.024E-08	9.614E-09
	9.822E+03	9.625E+03	**3.597E+04**	1.007E+04	1.015E+04	1.033E+04	9.678E-09	1.033E-08
	1.022E+04	1.045E+04	**1.750E+05**	9.625E+03	1.001E+04	9.574E+03	9.513E-09	9.978E-09
	9.793E+03	1.032E+04	**6.677E+06**	9.613E+03	1.045E+04	1.014E+04	1.027E-08	9.564E-09
	9.727E+03	9.721E+03	**7.356E+01**	9.678E+03	1.038E+04	1.002E+04	9.700E-09	9.855E-09
	1.040E+04	9.724E+03	**5.087E+06**	1.003E+04	9.654E+03	1.024E+04	9.740E-09	1.027E-08
	9.730E+03	9.670E+03	**3.744E+01**	9.765E+03	1.030E+04	1.003E+04	9.646E-09	9.862E-09
	9.843E+03	1.020E+04	**2.029E+04**	1.038E+04	9.662E+03	1.037E+04	1.006E-08	1.021E-08
	9.804E+03	9.629E+03	**6.041E+03**	1.007E+04	1.017E+04	9.984E+03	9.664E-09	1.038E-08
	1.016E+04	9.998E+03	**1.072E+01**	9.899E+03	1.024E+04	9.886E+03	1.007E-08	1.012E-08
S_4	9.894E+03	1.015E+04	1.042E+04	**4.974E+06**	1.033E+04	1.008E+04	1.030E-08	1.014E-08
	9.918E+03	9.593E+03	1.031E+04	**1.161E+02**	9.708E+03	1.029E+04	9.650E-09	1.027E-08
	1.003E+04	9.939E+03	9.806E+03	**1.224E+04**	1.011E+04	9.748E+03	1.048E-08	1.028E-08
	9.667E+03	1.023E+04	1.015E+04	**7.498E+03**	1.015E+04	1.033E+04	9.760E-09	1.008E-08
	9.913E+03	9.809E+03	9.887E+03	**6.015E+03**	1.031E+04	1.040E+04	1.011E-08	9.807E-09
	9.918E+03	9.655E+03	1.029E+04	**1.552E+01**	9.661E+03	1.030E+04	9.716E-09	1.027E-08
	9.684E+03	1.022E+04	9.770E+03	**4.216E+02**	9.986E+03	1.042E+04	9.753E-09	1.008E-08
	1.005E+04	9.957E+03	9.792E+03	**1.018E+06**	1.008E+04	9.752E+03	9.953E-09	9.876E-09
	1.004E+04	1.007E+04	9.902E+03	**4.345E+03**	1.032E+04	1.040E+04	1.012E-08	9.817E-09
	9.548E+03	1.007E+04	9.500E+03	**5.436E+05**	1.041E+04	9.994E+03	1.048E-08	1.033E-08
	9.696E+03	1.024E+04	1.018E+04	**8.571E+03**	1.017E+04	1.024E+04	1.015E-08	9.803E-09
	9.567E+03	1.002E+04	9.529E+03	**5.275E+04**	1.038E+04	9.994E+03	9.993E-09	9.870E-09
	9.947E+03	9.982E+03	1.009E+04	**9.630E+06**	1.034E+04	1.025E+04	9.571E-09	1.021E-08
	9.847E+03	1.040E+04	1.043E+04	**6.261E+05**	1.009E+04	1.004E+04	1.016E-08	1.011E-08
	1.003E+04	1.006E+04	9.857E+03	**2.110E+06**	9.685E+03	1.003E+04	1.005E-08	9.928E-09

the 2nd element 1.818E + 04Ω in vector $\boldsymbol{p}^*$ is out of the tolerance range, hence, the fault source is R_2. Fault diagnosis result is right.

C. ACTUAL EXAMPLE

In the following examples, the size of the subset is 30 and the maximum generation is 200. We use an actual CUT to verify the effectivity of the propose method in actual application. The experimental setup and CUT are shown in Fig. 2. The structure and parameters of the CUT are the same as those of the circuit shown in Fig.1. The excitation signals are $V_{p-p} =$ 5V sinusoidal waves with frequencies 500Hz, 1000Hz, and 1500Hz respectively. The DC source is ±12V.

When the circuit stimulated by the 1000Hz signal, the measured input signal and fault free voltages on the selected test point 'V*out*' are shown in figure 2. By comparing the two waves, it is easy to obtain the transfer function $H\ (j1000 \times 2\pi) = -0.7175 + j0.7332$. Now we randomly turn the adjustable resistance R3. The measured $\boldsymbol{H_M}$ are [−0.7906+j0.2084, −0.7526+j0.5250, −0.3946+j0.8953].

Then the proposed algorithm is used to obtain the optimal solution. The result is $\boldsymbol{p}^* = [9770\Omega, 9804\Omega, 7638\Omega, 10081\Omega, 9993\Omega, 10398\Omega, 10.03\text{nF}, 10.27\text{nF}]$. Obviously, the third element is out of the tolerance range. Fault diagnosis result is right.

D. STATISTICAL EXPERIMENT

To statistically check the accuracy of the proposed modeling method, on the bread board we respectively adjust each resistance and capacitance for 20 times. Totally, there are six resistances and two capacitances. The results of fault diagnosis are listed in Table 6. In this table, row represents the ambiguity sets and column is fault instance. If the fault instance is correctly fall into the corresponding ambiguity set, then the fault diagnosis is right. Take the fault instance R1 for example, it is correctly diagnosed by 19 times. While it is

TABLE 5. The final population P.

	R_1	R_2	R_3	R_4	R_5	R_6	C_1	C_2
	1.041E+04	1.818E+04	9.932E+03	9.715E+03	1.037E+04	1.030E+04	1.014E-08	1.016E-08
	1.048E+04	1.818E+04	9.984E+03	9.703E+03	1.037E+04	1.026E+04	1.015E-08	1.025E-08
	1.048E+04	1.818E+04	9.984E+03	9.671E+03	1.035E+04	1.025E+04	1.013E-08	1.014E-08
	1.049E+04	1.791E+04	9.971E+03	9.683E+03	1.034E+04	1.026E+04	1.016E-08	1.022E-08
	1.049E+04	1.791E+04	9.958E+03	9.720E+03	1.034E+04	1.026E+04	1.016E-08	1.014E-08
	1.047E+04	1.793E+04	9.985E+03	9.722E+03	1.032E+04	1.028E+04	1.016E-08	1.018E-08
	1.039E+04	2.615E+04	1.006E+04	9.663E+03	1.038E+04	1.028E+04	1.016E-08	1.016E-08
	1.039E+04	1.791E+04	9.957E+03	9.671E+03	1.034E+04	1.034E+04	1.022E-08	1.021E-08
	1.039E+04	1.818E+04	1.005E+04	9.624E+03	1.038E+04	1.022E+04	1.020E-08	1.012E-08
S_2	1.039E+04	1.818E+04	9.812E+03	9.845E+03	1.043E+04	1.034E+04	1.017E-08	1.023E-08
	1.042E+04	1.818E+04	9.890E+03	9.826E+03	1.042E+04	1.034E+04	1.006E-08	1.021E-08
	1.047E+04	1.793E+04	9.973E+03	9.664E+03	1.037E+04	1.028E+04	1.016E-08	1.024E-08
	1.042E+04	1.818E+04	9.890E+03	9.845E+03	1.031E+04	1.034E+04	1.015E-08	1.023E-08
	1.044E+04	1.793E+04	9.925E+03	9.722E+03	1.035E+04	1.027E+04	1.018E-08	1.021E-08
	1.042E+04	1.818E+04	9.766E+03	9.821E+03	1.045E+04	1.028E+04	1.017E-08	1.016E-08
	1.039E+04	1.242E+04	1.006E+04	9.624E+03	1.040E+04	1.030E+04	1.016E-08	1.020E-08
	1.048E+04	1.791E+04	9.957E+03	9.720E+03	1.034E+04	1.026E+04	1.016E-08	1.014E-08
	1.045E+04	1.793E+04	9.952E+03	9.722E+03	1.037E+04	1.028E+04	1.019E-08	1.021E-08
	1.044E+04	1.535E+04	9.914E+03	9.773E+03	1.040E+04	1.029E+04	1.015E-08	1.020E-08
	1.048E+04	1.822E+04	9.932E+03	9.763E+03	1.040E+04	1.027E+04	1.000E-08	1.017E-08
	1.039E+04	1.791E+04	9.957E+03	9.720E+03	1.034E+04	1.028E+04	1.016E-08	1.018E-08
	1.035E+04	1.818E+04	9.965E+03	9.773E+03	1.041E+04	1.036E+04	1.014E-08	1.021E-08
	1.046E+04	1.793E+04	9.977E+03	9.722E+03	1.035E+04	1.028E+04	1.016E-08	1.017E-08
	1.046E+04	1.793E+04	9.983E+03	9.703E+03	1.027E+04	1.026E+04	1.015E-08	1.025E-08
	1.047E+04	1.818E+04	9.909E+03	9.773E+03	1.035E+04	1.035E+04	1.011E-08	1.019E-08
	1.037E+04	1.818E+04	9.866E+03	9.808E+03	1.037E+04	1.025E+04	1.006E-08	1.026E-08
	1.041E+04	1.818E+04	9.890E+03	9.664E+03	1.031E+04	1.024E+04	1.016E-08	1.024E-08
	1.040E+04	1.436E+04	9.895E+03	9.722E+03	1.032E+04	1.028E+04	1.014E-08	1.017E-08
	1.040E+04	1.793E+04	9.973E+03	9.826E+03	1.042E+04	1.034E+04	1.006E-08	1.021E-08
	1.046E+04	1.818E+04	9.909E+03	9.773E+03	1.045E+04	1.036E+04	1.016E-08	1.019E-08
	1.043E+04	1.818E+04	9.875E+03	9.662E+03	1.026E+04	1.030E+04	1.015E-08	1.024E-08
	1.046E+04	1.818E+04	9.930E+03	9.838E+03	1.039E+04	1.030E+04	1.016E-08	1.024E-08
	1.042E+04	1.818E+04	9.880E+03	9.771E+03	1.049E+04	1.028E+04	1.018E-08	1.002E-08
	1.046E+04	1.793E+04	9.971E+03	9.674E+03	1.037E+04	1.028E+04	1.016E-08	1.016E-08
	1.048E+04	1.835E+04	9.908E+03	9.922E+03	1.038E+04	1.034E+04	1.008E-08	1.028E-08
	1.049E+04	1.791E+04	9.937E+03	9.635E+03	1.034E+04	1.027E+04	1.015E-08	1.020E-08
	1.046E+04	1.818E+04	9.899E+03	9.773E+03	1.041E+04	1.036E+04	1.014E-08	1.019E-08
	1.049E+04	1.791E+04	9.930E+03	9.846E+03	1.037E+04	1.022E+04	1.013E-08	1.024E-08
	1.049E+04	1.791E+04	9.979E+03	9.662E+03	1.031E+04	1.032E+04	1.015E-08	1.023E-08
	1.046E+04	1.818E+04	9.909E+03	9.773E+03	1.045E+04	1.036E+04	1.016E-08	1.019E-08

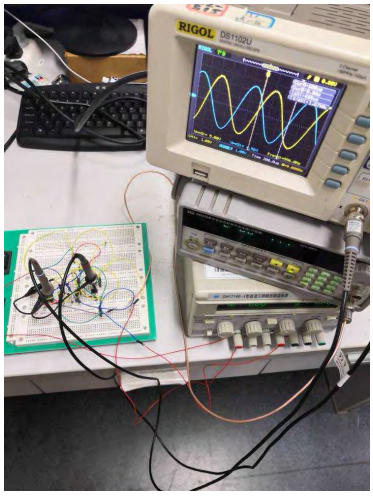

FIGURE 2. Experimental setup.

also improperly partitioned into set {R2} for one time. The reason is that the faulty value R1 = 10540Ω is very close to the tolerance border 10500Ω. In this scenario, the other fault free components' tolerance seriously affects the fault diagnosis accuracy. All R4 and C2 faulty instances are properly diagnosed.

TABLE 6. Actual fault diagnosis results.

	R_1	R_2	R_3	R_4	R_5	R_6	C_1	C_2
$\{R_1\}$	19	1	2	-	-	-	2	-
$\{R_2\}$	1	17	-	-	1	-	-	-
$\{R_3,C_1\}$	-	1	18	-	-	2	18	-
$\{R_4, R_5, R_6, C_2\}$	-	1	-	20	19	18	-	20
Rate(%)	95	85	90	100	95	85	85	100

Besides the actual experiments, we examine it on Monte Carlo simulations. For each fault source, 80 Monte Carlo simulations are executed; hence, 8 × 80 simulations are run. Not only the tolerance but also measurement error e = ±5% is taken into consideration. The Monte Carlo simulations are automatically accomplished by using MATLAB. To avoid the simulation divergence, the faulty value of cannot be 0. Hence the range of faulty parameter is $[N_0\times10^{-4}, N_0 \times 10^4]$, where N_0 is the nominal value. Take the R_1 in fig.1 for example,

TABLE 7. Simulated fault diagnosis results.

	R_1	R_2	R_3	R_4	R_5	R_6	C_1	C_2
$\{R_1\}$	78	0	3	-	1	-	4	-
$\{R_2\}$	-	77	-	-	2	2	-	-
$\{R_3,C_1\}$	-	0	77	-	-	-	67	-
$\{R_4, R_5, R_6, C_2\}$	2	3	0	80	77	78	9	80
Rate(%)	97.5	96.3	96.3	100	96.3	97.5	83.8	100

its faulty parameter range is $1 \sim 10^8\Omega$, where 1Ω and $10^8\Omega$ express short and open fault, respectively. Similarly, the parameter of a capacitance C_1 in fig.2 change between $10^{-12}\sim10^{-4}$F, where both ends represent open and short fault, respectively. The 8×80 sets of result are analyzed by using the proposed GA method. Table 7 shows that in most cases the accuracy is above 90 percent.

If all the components have the same fault rate, according the definition of fault resolution in [25], the proposed method has the following fault resolution.

$$FR_1 = \frac{78+77}{640} = 24.22\%$$
$$FR_2 = FR1 + \frac{78+77+77+67}{640} = 46.72\%$$
$$FR_3 = FR2 = 46.72\%$$
$$FR_4 = FR_3 + \frac{80+77+78+80}{640} = 95.94\%$$

By using the circle model [20], we have the same four ambiguity sets shown in Table 7. Because that the slope method [24] needs at least two test point, the Vout and the output port of the first operational amplifier are used to calculate the slope feature. This method partitions all the components into only two sets {R1,R2, R3, C1} with slope 0.0000-1.5915j and {R4, R5, R6, C2} with slope -1.0000-0.6283j. Obviously, the slope method need more test points while the fault resolution is low. The fault resolution results are listed in Table 8.

TABLE 8. Fault diagnosis accuracy.

	FR_1	FR_2	FR_3	FR_4
Slope model	0	0	0	93.86%
circle model	23.22%	47.72%	47.72%	94.73%
Proposed method	24.22%	46.72%	46.72%	95.94%

Table 8 shows that the slope model has the lowest fault resolution. The circle model and the proposed have the relative high accuracy. The advantage of the proposed method over the circle model is that the GA based method can realize both fault location and fault parameter identification while the circle model only realize fault location.

The slope model and circle model are SBT based methods. To obtain the fault signature and the influence of tolerance, the slope model needs $2 \times m$ simulations and the circle model needs $3 \times m$ simulations for each fault sources, where m is the number of Monte Carlo simulations. Usually, m = O(100). If there are n fault sources, the total simulation number is O($2mn$) = O(3mn) = O(mn) for both slope model and circle model based methods. If one simulation needs t seconds, the simulation time complexity is O(mnt). It grows dramatically with the increase of fault source number. While the proposed method does not need any SBT. The time complexity do not affect by either m or n. It needs about 2 seconds in fault diagnosis phase.

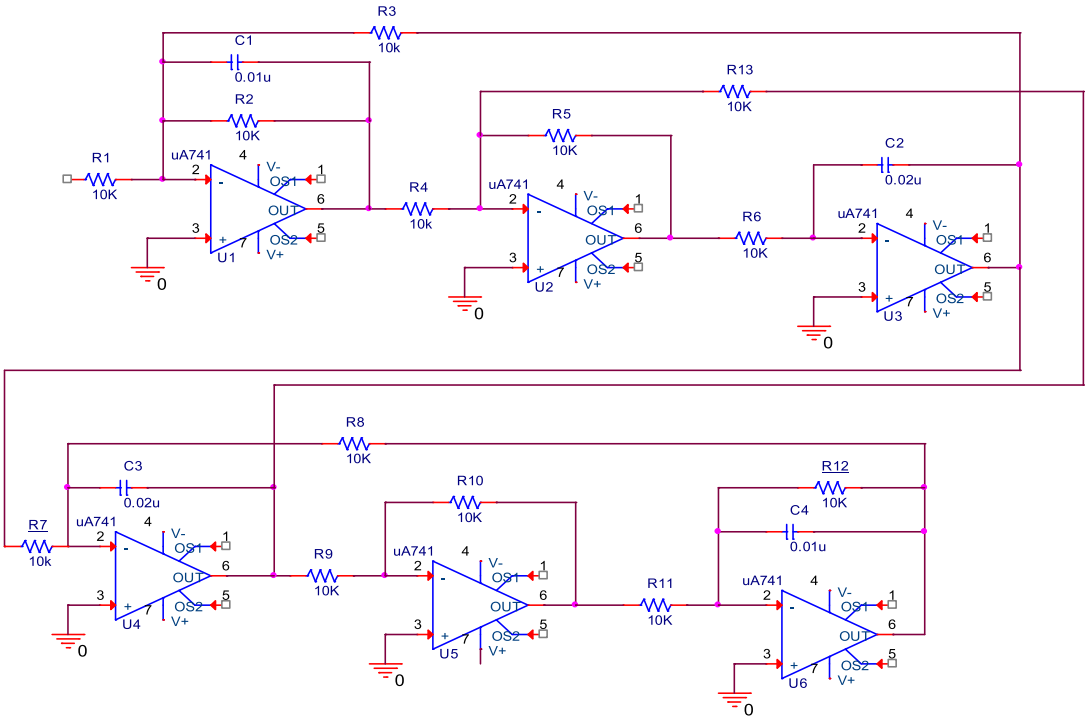

FIGURE 3. Leapfrog filter.

TABLE 9. Ambiguity set.

Ambiguous set	1	2	3	4	5	6	7	8	9	10	11
Fault component	R1	R2	R3	R4	R5, R6, C2	R7, R13	R8, R9, R10, R11	R12	C1	C3	C4

TABLE 10. Fault diagnosis results.

	R_1	R_2	R_3	R_4	R_5	R_6	R_7	R_8	R_9	R_{10}	R_{11}	R_{12}	R_{13}	C_1	C_2	C_3	C_4
$\{R_1\}$	96	9	2	0	0	0	0	0	0	0	0	0	0	0	0	0	0
$\{R_2\}$	4	84	2	0	0	0	0	0	0	0	0	0	0	0	0	0	0
$\{R_3\}$	0	7	86	0	0	0	5	0	0	0	0	0	0	0	0	0	0
$\{R_4\}$	0	0	0	100	0	0	0	0	0	0	0	0	0	6	0	0	0
$\{R_5, R_6, C_2\}$	0	0	0	0	91	85	0	0	0	0	1	0	0	5	89	0	0
$\{R_7, R_{13}\}$	0	0	10	0	0	0	95	82	73	81	78	72	93	0	0	0	0
$\{R_8, R_9, R_{10}, R_{11}\}$	0	1	0	0	0	0	0	13	13	6	5	2	0	0	0	0	10
$\{R_{12}\}$	0	0	0	0	9	0	0	3	0	8	2	6	0	0	0	0	12
$\{C_1\}$	0	0	0	0	0	7	0	0	0	0	0	0	0	89	11	0	0
$\{C_3\}$	0	0	0	0	0	8	0	1	12	5	1	13	7	0	0	100	0
$\{C_4\}$	0	0	0	0	0	0	0	1	2	0	0	7	0	0	0	0	78
Rate(%)	96	84	86	100	91	85	95	82	73	81	78	72	93	89	89	100	78

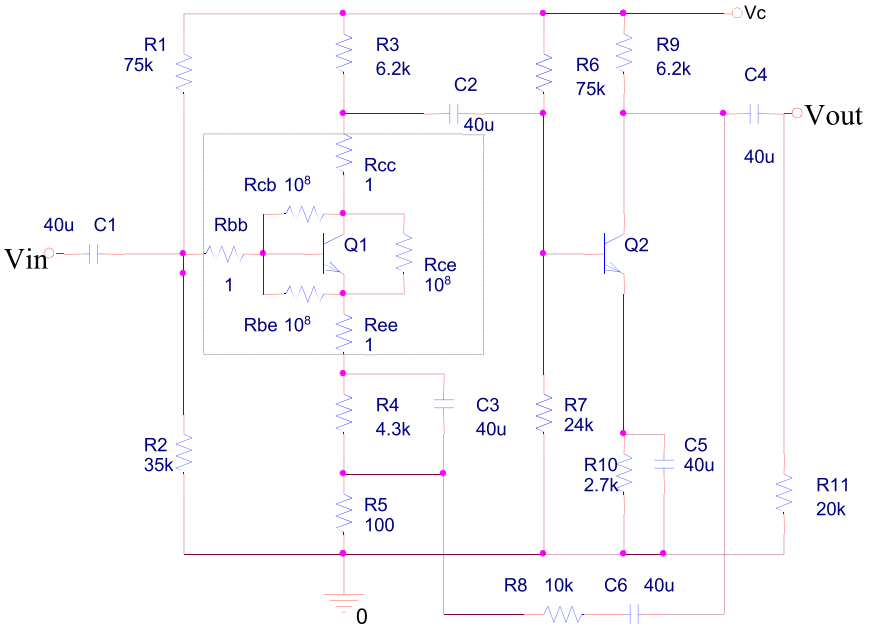

FIGURE 4. Negative feedback amplifier circuit.

The second statistical experiment is carried out on the leapfrog filter shown in figure 3. The test point is marked by 't'. Under the single fault assumption, the ambiguity set listed in Table 9 are obtained by using the method proposed in literature [24]. The range of faulty parameters and frequencies are same as that chosen in example 1. For each fault source, 100 Monte Carlo simulations are executed. In each simulation, the parameter of fault component varies within the faulty range $[N_0 \times 10^{-4}, N_0 \times 10^4]$. The faulty responses are used to guide the GA. The fault diagnosis results are listed in Table 10.

Table 9 shows that the proposed method can accurately find the fault source in most instances. All the R_4 and C_3 parameter and hard fault are 100% diagnosed. The R_9, R_{11}, R_{12} and C_4 have relative low fault diagnosis rate which is lower than 80%. Considering that the proposed method needs only one test point and it can diagnosis the wide range $[N_0 \times 10^{-4}, N_0 \times 10^4]$ of continues parameter fault (soft) and hard fault, the proposed method is a competitive method. Besides, the accuracy can be improved by selecting proper frequency or adding test point.

E. EXTENSION TO NONLINEAR CUT

This example is used to show that the proposed method is also applicable to nonlinear analog circuit. The explicit transfer function ($H(\boldsymbol{s}, \boldsymbol{p})$ shown in formula (1)) of nonlinear analog

TABLE 11.

	R_1	R_5	C_1	C_3	C_6
{R_1}	86	11	0	0	0
{R_5}	14	89	0	0	0
{C_1}	0	0	98	7	0
{C_3}	0	0	2	93	0
{C_6}	0	0	0	0	100
Rate(%)	86	89	98	93	100

circuit is hard to be obtained. In this case, the $H(\boldsymbol{s}, \boldsymbol{p})$ used in formula (2) is obtained by PSPICE simulation. We use MATLAB to control the PSPICE simulation. The simulation consists of three steps: adjusting the parameter values in netlist file according to the gene of individual, simulation and data loading. The experimental circuit is shown in Fig.4.

Usually, triode has three operation regions: cutoff, saturation and forward active regions. Different values of R1 may induce three different operation regions.

$$\begin{cases} R_1 < 125\Omega & \text{saturation region} \\ 125\Omega < R_1 < 39.8k\Omega & \text{active region} \\ 39.8k\Omega < R_1 & \text{cutoff region} \end{cases}$$

Hence the amplifier is a typical nonlinear circuit. The excitation (input) signals are 500Hz, 1kHz and 1.5kHz 10mV sinusoidal waves, and Vc = 5V. To simplify the analysis, 5 potential fault components R1, R5, C1, C3, and C6 are taken into consideration. For each fault source, 100 fault conditions, viz. 100 different fault values, are randomly generated, then the proposed GA is used to find the fault sources. Fault diagnosis results are listed in Table 10. It is need to point out that, in this example, the simulation analysis substitutes the transfer function, the time complexity is relative high.

V. CONCLUSION

Traditionally, analog circuit fault diagnosis has been carried out using simulation-before-test (SBT) strategies. The SBT method is easy to implement but this method cannot elaborately characterize all possible continues parameter shift fault occur in analog circuit. While based on the derived circuit transfer function equation, the simulation-after-test (SAT) can theoretically diagnose all parameter shifting faults. The proposed float encoding genetic algorithm can model all parameter shifting fault. Usually, the transfer function of linear CUT is obtainable. Lots of nonlinear analog components such as diode and triode are piecewise linear. The triode has three operation regions, based on the different quiescent operation point, we can write out three transfer functions corresponding to the three different operation regions. The proposed method is still executed efficiently. For the CUT without transfer function, to evaluate the fitness of an individual, the automatic simulation is an alternative method although it time complexity is higher than that of transfer function computation.

Different from the traditional GA, the proposed method partitions the populations into several groups based on the number of ambiguity sets. Any fault in a set can be chosen as the representative component. Each group represents a representative component. The crossover and mutation operation are executed within each group to insure the single fault situation. The selection operation is run with the whole populations to ensure the optimization. With the evolution, the group that represents the correct fault source is expanding while the size of other groups is shirking. Finally, all the individuals represent the correct fault source.

Summing up the above, the contributions of this paper includes two aspects. The first one is the analog fault diagnosis aspect: using the GA to emulate the parameter varying of analog circuit. The second aspect is GA itself: grouped crossover and mutation and integrated selection. The future work is to modify the GA to fit for double fault situation.

The main advantage of the proposed method is that it can diagnosis all parameter shift (soft) and hard faults without any SBT requirement. Besides, the non-faulty components' parameters are obtained at the same time. Its disadvantage is that if the transfer function is not available, the fault diagnosis time will increase.

REFERENCES

[1] Y. Yu, Y. Jiang, and X. Peng, "Multi-frequency test generation for incipient faults in analog circuits based on the aliasing measuring model," *IEEE Access*, vol. 6, pp. 34724–34735, 2018.

[2] H. Lei and K. Qin, "A general method for analog test point selection using multi-frequency analysis," *Analog Integr. Circuits Signal Process.*, vol. 84, no. 2, pp. 185–200, Aug. 2015.

[3] Y. Xie, X. Li, S. Xie, X. Xie, and Q. Zhou, "Soft fault diagnosis of analog circuits via frequency response function measurements," *J. Electron. Testing*, vol. 30, no. 2, pp. 243–249, 2014.

[4] J. J. Saucedo-Dorantes, M. Delgado-Prieto, R. A. Osornio-Rios, and R. de Jesus Romero-Troncoso, "Multifault diagnosis method applied to an electric machine based on high-dimensional feature reduction," *IEEE Trans. Ind. Appl.*, vol. 53, no. 3, pp. 3086–3097, May/Jun. 2017.

[5] L. Xu, M. Cao, B. Song, J. Zhang, Y. Liu, and F. E. Alsaadi, "Open-circuit fault diagnosis of power rectifier using sparse autoencoder based deep neural network," *Neurocomputing*, vol. 311, pp. 1–10, Oct. 2018.

[6] Y. Han, B. Tang, L. Deng, "Multi-level wavelet packet fusion in dynamic ensemble convolutional neural network for fault diagnosis," *Measurement*, vol. 127, pp. 246–255, Oct. 2018.

[7] Z. Liu, Z. Jia, C.-M. Vong, S. Bu, and J. Han, "Capturing high-discriminative fault features for electronics-rich analog system via deep learning," *IEEE Trans. Ind. Informat.*, vol. 13, no. 3, pp. 1213–1226, Jun. 2017.

[8] L. Penghua, C. Yi, C. Ming, Q. Yifeng, and Z. Ke, "Multiple fault diagnosis of analog circuit using quantum hopfield neural network," in *Proc. Chin. Control Decis., Conf.*, 2013, pp. 4238–4243.

[9] H. Zhao, H. Liu, W. Hu, and X. Yan, "Anomaly detection and fault analysis of wind turbine components based on deep learning network," *Renew. Energy*, vol. 127, pp. 825–834, Nov. 2018.

[10] Q. Ma, Y. He, and F. Zhou, "A new decision tree approach of support vector machine for analog circuit fault diagnosis," *Analog Integr. Circuits Signal Process.*, vol. 88, no. 3, pp. 455–463, 2016.

[11] Z. Zhang, Z. Duan, L. Yuan, and Y. Long, "A new swarm-SVM-based fault diagnosis approach for switched current circuit by using kurtosis and entropy as a preprocessor," *Analog Integr. Circuits Signal Process.*, vol. 81, no. 1, pp. 289–297, 2014.

[12] C. Zhang, Y. He, L. Yuan, W. He, S. Xiang, and Z. Li, "A novel approach for diagnosis of analog circuit fault by using GMKL-SVM and PSO," *J. Electron. Test.*, vol. 32, no. 5, pp. 531–540, Oct. 2016.

[13] M. Tadeusiewicz and S. Hałgas, "A method for local parametric fault diagnosis of a broad class of analog integrated circuits," *IEEE Trans. Instrum. Meas.*, vol. 67, no. 2, pp. 328–337, Feb. 2018.

[14] Q. Z. Zhou, Y. L. Xie, D. J. Bi, X. Xie, S. S. Xie, and X. F. Li, "Methodology and equipments for analog circuit parametric faults diagnosis based on matrix eigenvalues," *IEEE Trans. Appl. Supercond.*, vol. 24, no. 5, Oct. 2014, Art. no. 0601106.
[15] A. S. S. Vasan, B. Long, and M. Pecht, "Diagnostics and prognostics method for analog electronic circuits," *IEEE Trans. Ind. Electron.*, vol. 60, no. 11, pp. 5277–5291, Nov. 2013.
[16] Z. Liu, T. Liu, J. Han, S. Bu, X. Tang, and M. Pecht, "Signal model-based fault coding for diagnostics and prognostics of analog electronic circuits," *IEEE Trans. Ind. Electron.*, vol. 64, no. 1, pp. 605–614, Jan. 2017.
[17] M. Khanlari and M. Ehsanian, "An improved KFCM clustering method used for multiple fault diagnosis of analog circuits," *Circuits Syst. Signal Process.*, vol. 36, no. 9, pp. 3491–3513, Sep. 2017.
[18] A. Kumar and A. P. Singh, "Fuzzy classifier for fault diagnosis in analog electronic circuits," *ISA Trans.*, vol. 52, no. 6, pp. 816–824, 2013.
[19] M. Tadeusiewicz and S. Hałgas, "A new approach to multiple soft fault diagnosis of analog BJT and CMOS circuits," *IEEE Trans. Instrum. Meas.*, vol. 64, no. 10, pp. 2688–2695, Oct. 2015.
[20] M. Hu *et al.*, "Soft fault diagnosis for analog circuits based on slope fault feature and BP neural networks," *Tsinghua Sci. Technol.*, vol. 12, pp. 26–31, Jul. 2007.
[21] C. Yang, J. Yang, Z. Liu, and S. Tian, "Complex field fault modeling-based optimal frequency selection in linear analog circuit fault diagnosis," *IEEE Trans. Instrum. Meas.*, vol. 63, no. 4, pp. 813–825, Apr. 2014.
[22] S. Tian, C. Yang, F. Chen, and Z. Liu, "Circle equation-based fault modeling method for linear analog circuits," *IEEE Trans. Instrum. Meas.*, vol. 63, no. 9, pp. 2145–2159, Sep. 2014.
[23] K. Deb and R. B. Agrawal, "Simulated binary crossover for continuous search space," *Complex Syst.*, vol. 9, p. 115–148, Apr. 1995.
[24] G. Fedi, S. Manetti, M. C. Piccirilli, and J. Starzyk, "Determination of an optimum set of testable components in the fault diagnosis of analog linear circuits," *IEEE Trans. Circuits Syst. I, Fundam. Theory Appl.*, vol. 46, no. 7, pp. 779–787, Jul. 1999.
[25] *Testability Program for Electronic Systems and Equipments*, document MIL-STD-2165, 1985, pp. 55–56.

CHENGLIN YANG (M'17) received the Ph.D. degree in measurement technology and instruments from the University of Electronic Science and Technology of China, Chengdu, China. His current research interests include the multiobjective evolutionary algorithm, design for testability, fault diagnosis, and test generation. He was a recipient of the Best Paper Award of the IEEE Circuits and Systems Society in recognition of the excellence of his paper presented at the 2009 IEEE Circuits and Systems International Conference on Testing and Diagnosis. He was a Reviewer of the IEEE TRANSACTIONS ON INSTRUMENTATION AND MEASUREMENT and the *International Journal of Circuit Theory and Applications*.

LIU ZHEN (M'17) received the B.S. and M.S. degrees in electrical engineering from Northwestern Polytechnical University (NPU), Xi'an, China, in 1999 and 2002, respectively, and the Ph.D. degree in testing technology and automatic equipment from NWPU, in 2007. Since 2007, he has been with the University of Electronic Science and Technology of China (UESTC), where he is currently an Associate Professor with the Department of Instrument Science and Technology, School of Automation. He has been a leader or main member for several national research projects.

His research interests include testability analysis and design, fault diagnostic and fault prediction technology, and system reliability analysis technology.

CONG HU received the B.S. degree in computer science and technology and the M.S. degree in test and measurement technology and instruments from the Guilin University of Electronic Technology, Guilin, China, in 2003 and 2006, respectively, and the Ph.D. degree in test and measurement technology and instruments from Xidian University, Xi'an, China, in 2017. He is currently an Associate Professor with the Guilin University of Electronic Technology. His current research interests include design for testability, test optimization techniques for many-core designs, and fault diagnosis.